Water Research 269 (2025) 122771

Contents lists available at ScienceDirect

Water Research

journal homepage: www.elsevier.com/locate/watres

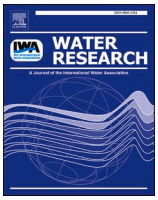

Modeling nitrogen recovery and water transport in gas-permeable membranes

C. Da Silva [a,*], A. Serra-Toro [a], V. Pelizzaro [b], F. Valentino [b], S. Astals [a], F. Mas [c], J. Dosta [a,d]

[a] Department of Chemical Engineering and Analytical Chemistry, University of Barcelona, Barcelona 08028, Spain
[b] Department of Environmental Sciences, Informatics and Statistics, Ca' Foscari University of Venice, Mestre, Venice 30170, Italy
[c] Materials Science and Physical Chemistry Department & Research Institute of Theoretical and Computational Chemistry (IQTCUB), University of Barcelona, Barcelona 08028, Spain
[d] Water Research Institute, University of Barcelona, Barcelona 08001, Spain

ARTICLE INFO

Keywords:
Fertilizer
Hydrophobicity
Membrane
Nitrogen recovery
Osmotic pressure

ABSTRACT

This study presents a new modeling approach for nitrogen recovery in gas-permeable membrane (GPM) contactors, including both ammonia and water transport dynamics. A distinct feature of the model is its capacity to model water transport across the membrane, which has been overlooked in most publications. Osmotic pressure differences are used to predict the behavior of ammonia and water transport in the GPM contactor. Experiments carried out to develop, test and calibrate the model examined the dynamics of ammonia and water transport through the GPM contactor at various nitrogen concentrations. Specifically, the GPM contactor was tested for nitrogen recovery from high-strength synthetic wastewaters (2.4–10.6 g N/L) at 35 °C and at pH 9. The initial volume of the trapping solution (diluted H_2SO_4) was 10 times lower than that of the synthetic wastewater, aiming to concentrate the recovered nitrogen. The estimated ammonia transport constant (K_m) ranged between (1.2 - 2.1)·10^{-6} m/s and water transport constant K_w between (2.8 - 8.2)·10^{-10} m/(s bar). Numerical determination of the model parameters revealed high R^2 values, demonstrating strong agreement with experimental data.

1. Introduction

Nitrogen pollution is a critical environmental issue that arises from agricultural, industrial, and domestic activities (de Vries, 2021). The production of ammonia through the Haber-Bosch process is highly energy-intensive, consuming around 6.4·10^{12} MJ/year worldwide. This accounts for approximately 2 % of the world's total energy consumption and 0.93 % of global greenhouse gas emissions (Rizzioli et al., 2023). Ammoniacal nitrogen, sum of ammonia (NH_3) and ammonium ion (NH_4^+), is a major polluter of aquatic systems that causes eutrophication, which results in excessive growth of aquatic plants, deterioration of water quality, and threats to aquatic biodiversity (Rongwong and Sairiam, 2020). Wastewaters are the primary sink of wasted nitrogen (Noriega-Hevia et al., 2023). Therefore, the recovery of ammoniacal nitrogen present in wastewaters represents a solution to mitigate its impact in the environment while contributing to meet the growing demand for fertilizers within the framework of the circular economy (de Vries, 2021).

Various technologies have been developed to recover and remove nitrogen from wastewater, including biological and physico-chemical processes (Beckinghausen et al., 2020; Daguerre-Martini et al., 2018; de Vries, 2021). Biological processes, such as nitrification and denitrification, convert ammoniacal nitrogen into inert nitrogen gas but do not allow for its recovery. This process also requires significant energy and large reactor volumes (Rongwong and Sairiam, 2020). Physico-chemical processes, such as ammonia stripping, struvite crystallization, and ion exchange, have limitations related to efficiency, operational costs, and complexity (Aguilar-Pozo et al., 2023; Al-Juboori et al., 2022; Licon Bernal et al., 2016; Noriega-Hevia et al., 2023).

Membrane technologies have also been researched to recover nitrogen from wastewaters with promising results (Al-Juboori et al., 2022; Beckinghausen et al., 2020). Among them, gas-permeable membrane (GPM) contactors stand out due to their simple operation, low energy consumption (ca. 0.18 kWh per kg of NH_3 recovered), and operation at low pressure (Riaño et al., 2019). GPM technology operates by allowing the transfer of ammonia gas through a hydrophobic membrane into an

* Corresponding author.
E-mail address: cristopher.dasilva@ub.edu (C. Da Silva).

https://doi.org/10.1016/j.watres.2024.122771
Received 26 July 2024; Received in revised form 18 October 2024; Accepted 7 November 2024
Available online 8 November 2024

acidic solution on the other side, where it reacts to form a concentrated ammonium salt solution (Munasinghe-Arachchige et al., 2021). By keeping the pH of the feed solution at alkaline conditions (the pKa of NH_3 at 25°C is 9.26), the formation of gaseous ammonia is favored. The ammonia gas then diffuses through the air-filled pores of the hydrophobic membrane towards the acidic side, where it is trapped as ammonium ion (Munasinghe-Arachchige et al., 2021). This process operates effectively under ambient temperature and pressure conditions, making it an attractive solution with low energy demands and high product quality (Darestani et al., 2017; Dube et al., 2016).

High nitrogen recovery efficiencies (around 98 %) have been achieved by GPM contactors for the treatment of waste streams, including municipal wastewater, pig slurry, human urine and anaerobic digestion supernatants (Beckinghausen et al., 2020; Noriega-Hevia et al., 2023; Xie et al., 2016; Zhang et al., 2020). However, there a some challenges that limit widespread adoption of GPM technology for nitrogen recovery, including wetting, membrane fouling and the need for chemical additives to maintain pH levels during the process (Licon Bernal et al., 2016; Mosadegh-Sedghi et al., 2014; Rizzioli et al., 2023; Rongwong and Sairiam, 2020). The wetting of membrane pores has a significantly impact on mass transfer coefficients of the membrane, resulting in a sharp increase in membrane resistance to ammonia transport (Mosadegh-Sedghi et al., 2014; Rongwong and Sairiam, 2020). Fouling obstructs the nanopores while reducing the hydrophobicity of the membrane, which hinders ammonia transport and limits the scalability of the process (Licon Bernal et al., 2016). Despite these challenges, continuous advancements in membrane materials and process optimization could mitigate the extent of these barriers and enhance the efficiency and economic feasibility of GPM technology for nitrogen recovery. Several strategies have been researched to overcome fouling and wetting challenges, including (i) increasing feed flow rates to induce turbulence and reduce fouling; (ii) periodic cleaning with diluted acids or alkaline solutions to restore membrane performance after prolonged use (Al-Juboori et al., 2023); (iii) advances in material technology, including the development of superhydrophobic membranes, and specialized coatings to enhance hydrophobicity (Al-Juboori et al., 2023; Li et al., 2007). These advances potentially improve the efficiency and economic viability of GPM systems for nitrogen recovery.

Another important limitation of GPM technology is the transport of water through the membrane, which dilutes the trapping solution and reduces its economic value (Al-Juboori et al., 2022; Sheikh et al., 2023). Accordingly, modeling both nitrogen and water transport in ammonia selective membranes is crucial to understand nitrogen recovery in GPM contactors. This knowledge allows adjusting operational parameters to optimize the efficiency and viability of the process. Some publications attribute the transport of ammonia across the membrane to a difference in vapor pressure between the two sides of the membrane (Eq. (1)) (Gonzalez-Salgado et al., 2023; Rongwong and Sairiam, 2020; Sheikh et al., 2023). However, most publications explain the transport of ammonia as the result of a concentration gradient (Eq. (2)) (Norddahl et al., 2006; Serra-Toro et al., 2022a; 2024). The gradient in ammonia vapor pressures can be transformed into a gradient in ammonia concentrations as described in Sheikh et al. (2023).

$$j_{NH_3} = \frac{K_m}{R \cdot T} \cdot \left(p_{NH_3,f} - p_{NH_3,t} \right) \tag{1}$$

Where j_{NH_3} is the ammonia flux across the membrane, K_m is the mass transfer coefficient, $\left(p_{NH_3,f} - p_{NH_3,t} \right)$ is the difference of ammonia vapor pressure between the feed and the trapping solution chambers, T is the temperature, and R the ideal gas constant.

$$j_{NH_3} = K_m \cdot \left([N_{NH_3}]_f - [N_{NH_3}]_t \right) \tag{2}$$

Where $\left([N_{NH_3}]_f - [N_{NH_3}]_t \right)$ is the difference of ammonia concentration between the feed and the trapping solution chambers.

The transport of water molecules across the membrane is caused by the gradient of water chemical potential, which depends on the water activity (a_w) (Baker, 2023). However, obtaining simple expressions for water activity that are suitable for modeling purposes is difficult due to the lack of formulas in literature (Ott and Boerio-Goates, 2000; Sheikh et al., 2023). One approach to describe water flux is from vapor pressure gradient, even though its calculation uses a water activity estimation (Rongwong and Sairiam, 2020; Sheikh et al., 2023). Then, this transport can be modelled from water vapor pressure differences (Eq. (3)) (Al-Juboori et al., 2022).

$$j_w = K'_w \cdot \left(p_{w,f} - p_{w,t} \right) \tag{3}$$

Where j_w is the water flux across the membrane, K'_w is the mass transfer coefficient, and $\left(p_{w,f} - p_{w,t} \right)$ is the water vapor pressure difference between the feed and the trapping solution chambers.

Another way to obtain water activity is from osmotic pressure (Eq. (4)) (Baker, 2023), which is easier to measure experimentally or estimated by using the osmotic coefficient (ϕ) as a correction to total solute concentration in the van't Hoff's ideal expression (Atkins et al., 2022; Berk, 2009). Then, the water flux across the membrane could be related with the difference of osmotic pressures between the two sides of the membrane.

$$\Delta\pi = -\frac{R \cdot T}{V_w^*} \cdot \Delta(\ln a_w) \cong R \cdot T \cdot \Delta\left(\phi \cdot \sum_i [s_i] \right) \tag{4}$$

Where V_w^* is the molar volume of water, ϕ is the osmotic coefficient of the solution (feed or trapping), and $[s_i]$ is the concentration of each solute species (feed or trapping).

The objective of this study is to develop a predictive model for the transport of ammonia and water in gas-permeable membrane contactors. By understanding the dynamics of both ammonia and water transport across the membrane, this model aims to be a useful tool to optimize the operational conditions and to predict the dilution effect that could compromise the quality or commercial value of the generated trapping solution.

2. Materials and methods

2.1. Experimental design

Fig. 1 illustrates the experimental set-up of the GPM contactor used for recovering ammoniacal nitrogen, hereafter total ammoniacal nitrogen (TAN). The feed-to-trapping chambers volume ratio in these experiments was 10:1. Two sealed and jacketed tanks equipped with a magnetic stirrer (IKA C-MAG HS7) and a thermostatic bath to control the temperature at 35 °C (Thermo Scientifc HAAKE DC30) were used as chambers for the feed and the trapping solution. The temperature of the tanks was maintained at 35 °C by circulating water from a thermostatic bath through the jacket of the tanks. The synthetic feed solution (5.0 L) consisted of deionized water with NH_4Cl to reach the desired TAN concentration (i.e. 2.4, 5.2, 7.1 and 10.6 g N/L) and 5.0 g/L of acetic acid, while the acidic trapping solution (0.5 L) initially contained H_2SO_4 at 1 % in weight. Both solutions were circulated at a flow rate of 12 L/h

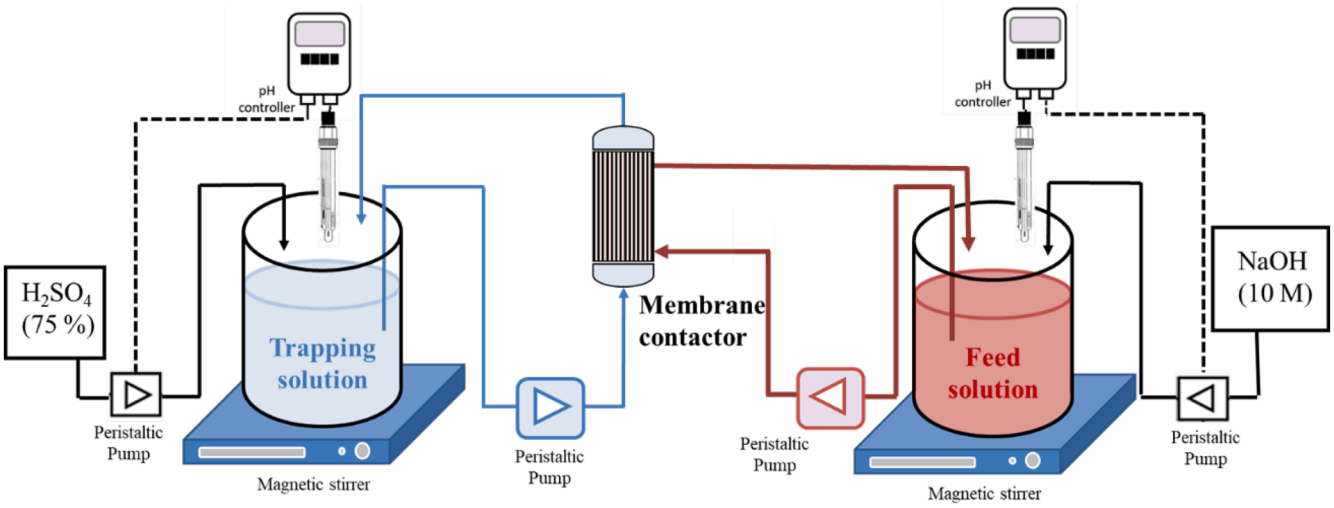

Fig. 1. Experimental set-up of the gas-permeable membrane contactor.

using a peristaltic pump (Masterflex L/S models 7518–12) in a closed loop configuration to the microporous hollow-fiber polypropylene membrane contactor (3M, 1.7 × 5.5 MiniModule). The GPM contactor had an active surface area of 0.50 m^2. Each tank was also equipped with a pH control system, comprising a pH electrode (Crison, code 53 35) and a pH controller (Crison, pH 28) connected to peristaltic pumps (Ismatec, Type ISM827) that added NaOH 8 M and H_2SO_4 25 % to the feed and trapping solution, respectively. The trapping solution was kept at an average pH of 1, sufficiently acidic to retain the diffused NH_3 as NH_4^+ since charged species cannot diffuse through the membrane. Conversely, the feed solution was kept at a pH 9 to displace the TAN equilibrium towards NH_3 since only uncharged species can diffuse across the membrane (Serra-Toro et al., 2022b).

Experiments were monitored by collecting multiple samples from both the feed and trapping solutions over the course of 50 h. Samples were taken hourly for the first 8 h, with two samples collected during the first hour. Each sample involved withdrawing 4 mL from each solution, which was then stored at 4 °C until TAN analysis. The volume of the feed and trapping were determined using a millimeter graph paper that correlated the liquid height with the volume in each tank. The consumption of reagents for pH control was also monitored to account for volume changes due to water diffusion. TAN concentrations were measured with a Thermo Fisher Scientific ion-selective electrode (Orion 9512HPBNWP) according to procedure 4500-NH3D. Acetic acid was analyzed using a Shimadzu GC-2010 plus gas chromatograph equipped with an Agilent DB-FFAP capillary column and flame ionization detector (Perez-Esteban et al., 2024). All the experiments and measurements carried out in this study were done by duplicate.

2.2. Data curation

To quantify the volume of water that diffused through the membrane, a correction of the experimental values was needed to keep the total volume constant throughout the experiment. Specifically, the volume corresponding to the addition of reagent was subtracted to the total volume (which value was obtained from the calibrated mark), and the volume extracted in each sampling event to monitor the process was added. This correction allowed to only account for volume variations caused by water passage. There was a discrepancy between experimental and theoretical TAN concentration in the trapping solution, which could be attributed to TAN measurements error or ammonia volatilization, among others. To overcome this discrepancy, TAN concentrations in the trapping solution were estimated by a nitrogen mass balance (Eq. (5)). Parameters used to infer this concentration were the chamber volumes and the TAN concentration in the feed solution.

$$TAN_{trapping} = \frac{V_{feed_0} \cdot TAN_{feed_0} - V_{feed} \cdot TAN_{feed}}{V_{trapping}} \quad (5)$$

Where index *0* means initial, *V* means volume (L) and *TAN* means concentration (g N/L).

To calculate the osmotic pressure in the feed and trapping chambers, it is necessary to estimate the concentrations of all the species present in both solutions, including H^+, OH^-, NH_4^+, NH_3, Na^+, SO_2^{4-}, Cl^-, and acetate. The amount of NaOH and H_2SO_4 added to control the pH were estimated based on the concentration that ensured the electroneutrality in each chamber. This correction was proposed because the experimental set-up involved discrete additions of NaOH and H_2SO_4, while peak additions could affect the model. In the feed solution (pH = 9), it was considered that the concentrations of H^+ and OH^- were negligible compared to TAN, Cl^-, Na^+ and acetate. The Cl^- and acetate concentrations were calculated from the initial amount of NH_4Cl and acetic acid in the feed solution. The NH_4^+ and NH_3 concentrations were calculated combining the experimental TAN concentration, the pK_a at 35 °C, and the activity coefficient from the Davies equation (Supplementary Material, Section A), based on ionic strength from the electroneutrality condition. In the trapping chamber, the pH was controlled at an average value of 1. Therefore, the ions present were SO_4^{2-}, NH_4^+, and H^+. The concentrations of H^+ and SO_4^{2-} were estimated combining the electroneutrality condition and pH value, correcting the H^+ activity coefficient (Supplementary Material, Section A). The NH_4^+ concentration of the trapping chamber was the concentration that fulfilled the nitrogen mass balance.

The time-dependent osmotic pressure of both chambers was calculated considering the concentrations of all species in every sampling event. The osmotic pressure was calculated using a corrected version of the van't Hoff equation, along with an estimated osmotic coefficient for each solution (Tables of osmotic coefficients can be found in the Supp Material, Section A).

2.3. Parameter estimation using a conventional model not considering water passage

The model shown in Eq. (6) estimates ammonia diffusion with no water transport across the membrane (Licon Bernal et al., 2016; Serra-Toro et al., 2022b; Vecino et al., 2019; Zhu et al., 2005). A detailed deduction of this equation is provided in the Supplementary Material, Section B.

$$TAN_f = TAN_{f,0} \cdot \exp\left(-\frac{K_m \cdot A}{V_f} \cdot t \right) \quad (6)$$

If the volumes of the feed and the trapping solution remain constant, by nitrogen mass balance, the TAN in the trapping solution can be calculated using Eq. (7).

$$TAN_t = \frac{(TAN_{f,0} - TAN_f) \cdot V_f}{V_t} \quad (7)$$

Where TAN_f represents the TAN concentration in the feed solution over time (g N/L), $TAN_{f,0}$ is the initial TAN concentration in the feed (g N/L), K_m is the nitrogen mass transfer coefficient (m/s), A is the surface area of the membrane (m^2), V_f is the volume of the feed assumed to be constant (m^3), V_t is the volume of the trapping, assumed to be constant (m^3), t is time (s), and TAN_t is the TAN concentration in the trapping solution chamber over time (g N/L). Eq. (6) describes the exponential decay of TAN concentration in the feed solution and has been extensively used to estimate nitrogen transfer coefficients in GPM contators. Eq. (7) estimates the TAN concentration in the trapping chamber using the mass balance principle.

The K_m from Eq. (6) was obtained using the least-squares method, the *lsqnonlin* function, and the 'trust-region-reflective' optimization algorithm in MATLAB (R2023a), with a default tolerance of $1 \cdot 10^{-10}$. This method minimizes the mean-squared discrepancies between the collected experimental data and the model predictions for the feed chamber.

2.4. Development of a new model for GPM contactors considering water transport

In the proposed model, the transport of ammoniacal nitrogen and water are predicted using a mass balance for each compartment at both sides of the membrane (feed and trapping solution, Fig. 2). This balance assumes that the volume of the feed and trapping chamber are variable, resulting in four mass balances: two for modeling NH_3 transport and two for modeling water transport. For the NH_3 transport, an equation is formulated where the driving force is the difference in TAN concentrations based on first Fick's Law (Sheikh et al., 2023). The TAN mass balance in the feed chamber is shown in Eq. (9) obtained by developing Eq. (8). Similarly, the TAN mass balance for the trapping solution compartment is presented in Eq. (10).

$$\frac{d([TAN]_f \cdot V_f)}{dt} = -K_m \cdot A \cdot \left([N_{NH_3}]_f - [N_{NH_3}]_t \right) \quad (8)$$

$$\frac{d(TAN_f)}{dt} = \frac{1}{V_f} \cdot \left(TAN_f \cdot \frac{dV_f}{dt} - K_m \cdot A \cdot \left([N_{NH_3}]_f - [N_{NH_3}]_t \right) \right) \quad (9)$$

$$\frac{d(TAN_t)}{dt} = \frac{1}{V_t} \cdot \left(TAN_t \cdot \frac{dV_t}{dt} + K_m \cdot A \cdot \left([N_{NH_3}]_f - [N_{NH_3}]_t \right) \right) \quad (10)$$

Water transport was modeled using a water mass balance and assuming a constant density of water, where the driving force was represented by the difference in osmotic pressure between both sides of the hydrophobic membrane. Eqs. (11) and (12) are the water diffusion equations for the feed and the trapping chambers, respectively.

$$\frac{dV_f}{dt} = -K_w \cdot A \cdot (\pi_t - \pi_f) \quad (11)$$

$$\frac{dV_t}{dt} = K_w \cdot A \cdot (\pi_t - \pi_f) \quad (12)$$

Where V is the water volume in the chamber (L), TAN is the ammoniacal nitrogen concentration (g N/L), A is the membrane area (m^2), K_m is the NH_3 permeability constant (m/s), K_w is the water permeability constant (m/(s bar)), and π is the osmotic pressure (bar). The index f and t refer to the feed and trapping solution, respectively.

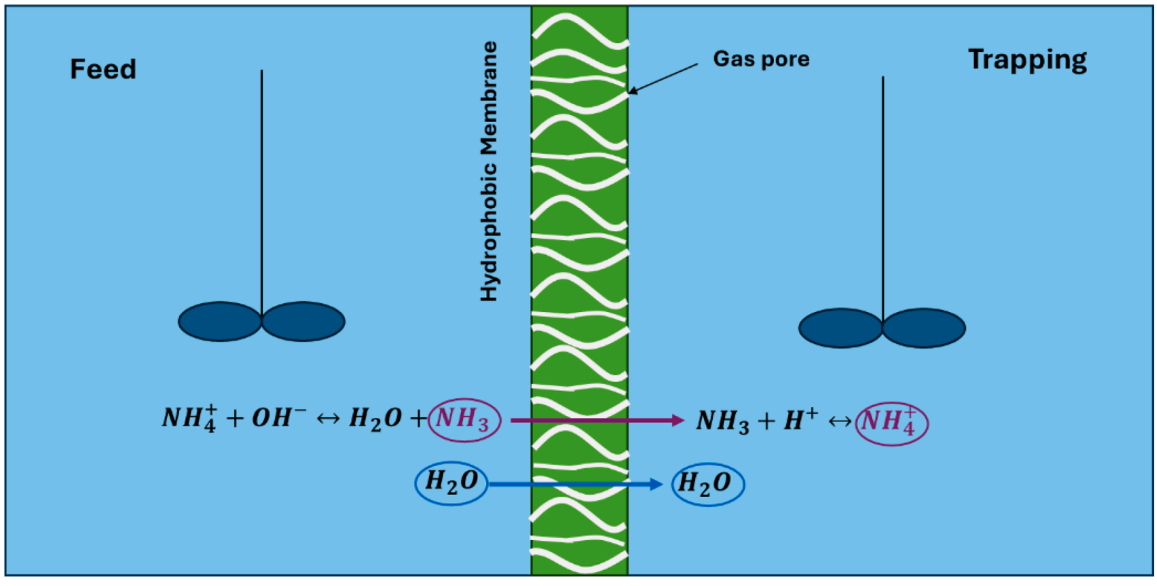

Fig. 2. Diagram of membrane contactor and species relevant to the model including water transport.

The ammonia concentration $[N_{NH_3}]$ in the feed and trapping solution was estimated by assuming that the equilibrium between ammonium ion and dissolved free ammonia is rapidly reached in each compartment. Assuming an equilibrium state scenario for ammonium-ammonia system, the dissolved N_{NH_3} concentration was estimated by using equilibrium relationships (Tchobanoglous et al., 2014), neglecting the activity coefficients as for Eqs. (13) and (14).

$$\left[N_{NH_3}\right]_f = TAN_f \cdot \frac{10^{pH_f}}{\frac{1}{K_a} + 10^{pH_f}} \tag{13}$$

$$\left[N_{NH_3}\right]_t = TAN_t \cdot \frac{10^{pH_t}}{\frac{1}{K_a} + 10^{pH_t}} \tag{14}$$

Where the equilibrium constant is a function of temperature (Eq. (15)), where T is the temperature in°C.

$$K_a = \exp\left(-\frac{6334}{273+T}\right) \tag{15}$$

2.5. Parameter estimation of the proposed model with differential equations considering water transport

The parameters (**p**) estimation problem is formulated as a nonlinear least squares optimization (Tesser and Russo, 2020). The objective function (S) is constructed to minimize the sum of squared residuals, defined as the difference between the experimental data and the predicted by the differential system of ordinary differential equations (ODEs) model (**y**):

$$\begin{array}{l} S(\boldsymbol{y},\boldsymbol{p}) \\ \boldsymbol{p},\ \boldsymbol{y} \\ s.t.: \dot{\boldsymbol{y}} = \boldsymbol{f}(\boldsymbol{y},\boldsymbol{p}) \end{array} \tag{16}$$

With:

$$S(\boldsymbol{y},\boldsymbol{p}) = \sum_{model,j=1}^{4} \sum_{i=1}^{n} \left(\frac{\left(y_{exp,ij} - y_{i,j}(p)\right)}{max\left(y_{exp,j}\right)} \right)^2 \tag{17}$$

The objective function (Eq. (17)) divides the residuals by the maximum value of the experimental variable. This normalization ensures that the objective functions are scaled between zero and one, thus enabling an effective global minimization. This normalization yields similar importance to all objective functions being minimized, contributing to a more balanced and representative optimization of all involved variables (Marler and Arora, 2010; Soto et al., 2017).

The optimization is carried out using the 'lsqnonlin' function in MATLAB 2023, employing the 'trust-region-reflective' algorithm. The confidence intervals for the optimized parameters are estimated using the 'nlparci' function, which computes the intervals based on the residuals and the Jacobian matrix obtained from 'lsqnonlin'. The integration of the model is performed with initial conditions from the experimental data. The system of differential equations is solved using the 'ode23' solver in MATLAB, which numerically integrates the equations over the time span of the experimental data. To evaluate the model fit, the coefficient of determination (R^2) is calculated for each variable (Eq. (18)).

$$R^2 = 1 - \frac{variance\left(residuals_j\right)}{variance\left(experimental\ data_j\right)} \tag{18}$$

3. Results and discussion

3.1. Results from the conventional model without water transport

Fig. 3 shows the evolution of TAN in the feed and the trapping solution for the experiments carried out at 2.4, 5.2, 7.1 and 10.6 g N/L. Fig. 3 shows that the TAN concentration in the trapping solution reached a peak concentration after about 10 h of experimentation and then progressively decreased. This occurred despite the continued nitrogen transfer, as highlighted by the TAN concentration decrease in the feed solution. The decrease in TAN concentration in the trapping solution was directly related to the transport of water across the membrane. Acetic acid was not detected in the trapping solution. Hence, this species was not capable of diffusing through the membrane under these conditions. Water diffusion across the membrane was caused by the appearance of a driving force between both sides of the hydrophobic membrane.

The conventional model for ammonia diffusion without considering water transport (Eq. (6)) could represent the TAN concentration in the feed chamber (Fig. 3). Nonetheless, the conventional model overestimated the TAN concentration in the trapping solution when the water passage becomes more notable. Table 1 reports the K_m values obtained from fitting the TAN concentration in the feed chamber using the conventional model for GPM contactors.

The fitting of the TAN concentration in the feed chamber using the conventional model without water transport (Eq. (6)) yields a high R^2, as the model closely matches the experimental data. Water transport had a lower effect on the TAN concentrations in the feed chamber. However, it had a greater effect in the TAN concentration of the trapping chamber, where the diluting effect was larger (Fig. 3). Indeed, the TAN concentration predictions in the trapping chamber overestimated the actual value. This discrepancy indicates that, in addition to ammonia transport, water transport also occurred, resulting in dilution of the trapping solution. A diluted trapping solution is a limitation for the feasibility of the process since achieving a highly concentrated solution is needed for both technical applications and product marketability. The K_m values obtained in this study (Table 1) were within the reported range from literature studies: $3.0 \cdot 10^{-7}$ m/s (Serra-Toro et al., 2024), $(4.0–0.6) \cdot 10^{-7}$ m/s (Licon Bernal et al., 2016) and $(1.2–2.4) \cdot 10^{-6}$ m/s (Noriega-Hevia et al., 2020). This simplified model accurately describes nitrogen recovery using GPM contactors, based on the assumption that the volumes of the feed and trapping solution do not change due to water transport in a closed loop configuration. However, for those cases where the working volume of the feed and/or the trapping solution is significantly affected, the final concentration of the trapping solution could not be accurately predicted. In the latter scenario, water transport must be considered in the model to predict the TAN concentration in the trapping chamber.

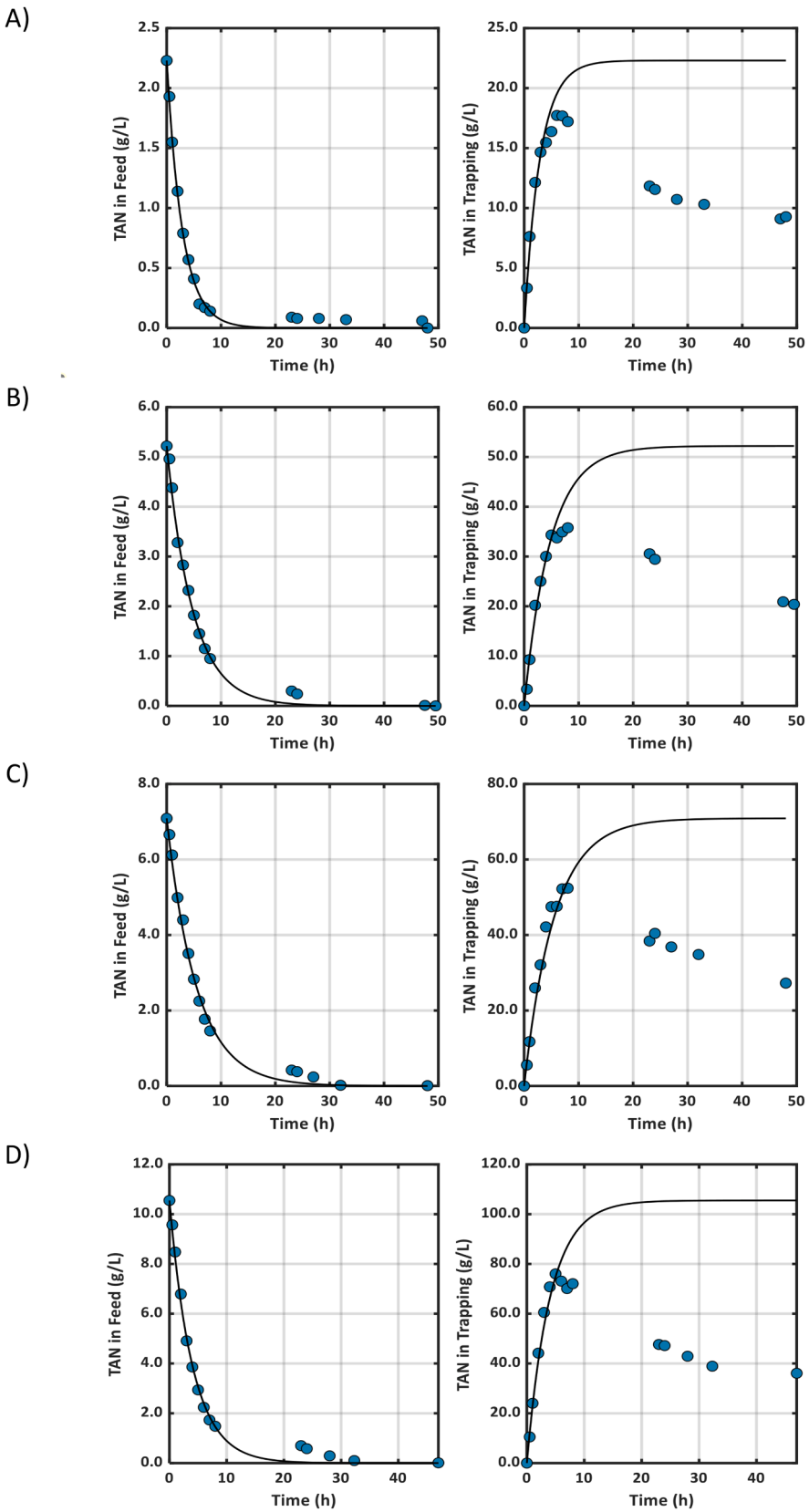

Fig. 3. Fitting results of experimental data (dots) for the model without water transport (line) at different feed solution TAN concentrations: A (2.4 g N/L), B (5.2 g N/L), C (7.1 g N/L), and D (10.6 g N/L).

3.2. Results from the new model considering water transport

Figs. 4–7 show the evolution of TAN and the volume change in both the feed and the trapping solution chambers as well as the fit obtained with the new model. The predicted model parameters (Table 2), K_m and K_w, showed little variability while maintaining low error margins and remaining within the same order of magnitude for the four experiments (different starting feed solution TAN concentration). The K_m values were slightly higher than those predicted using the conventional model without considering water transport (Table 1). The higher K_m values obtained with the new model was due to the reduction of the feed volume chamber.

The K_w obtained from fitting the experimental data was $(2 - 8)\cdot10^{-10}$ m/(s bar). This value could not be directly compared with other values reported in literature since the proposed model uses osmotic pressure differences to model the driving force for water transport instead of the vapor pressure difference (Sheikh et al., 2023). However, the average water fluxes could be compared with other studies reported in scientific literature. The average water fluxes values obtained at 50 h of operation were 0.026 ± 0.005, 0.028 ± 0.004, 0.027 ± 0.004 and 0.035 ± 0.008 kg/(m² h) for the experiments carried out at 2.4, 5.2, 7.1 and 10.5 g N/L, respectively. During the first 2 h of operation, water fluxes ranged between −0.050 and −0.05 kg/(m² h), with the negative values indicating water diffusion from the trapping solution to the feed solution due to the higher osmotic pressure of the feed solution. This effect was also observed when recording the volume the volume of the trapping solution over time, which slightly decreased during the first 2–4 h of operation and then increased (Figs. 4–6). The maximum water fluxes reached values from 0.050 to 0.085 kg/(m² h) when the concentration gradient between solutions was higher. Further details regarding flux variation over time can be found in Section C of the Supplementary Material.

Average water fluxes of 22.1 ± 6.1 kg/(m² h) were reported by Sheikh et al. (2023) when working with PP-LLMC and PMP-LLMC membranes. Fillingham et al. (2017) reported average water fluxes between 0.14 and 0.05 kg/(m² h) when working with a polytetrafluoroethylene membrane. In this study, the relatively low water transport through the membrane (0.050 to 0.085 kg/(m² h)) may explain the highly pronounced maximum TAN concentration observed in the trapping solution. High water transport is an undesirable phenomenon for GPM contactors because it limits the build-up of TAN concentration in the trapping solution, lowering its commercial value (Sheikh et al., 2023).

A good fit between the experimental data and the model predictions was obtained as indicated by high R^2 values for the volumes and TAN in the feed and trapping solution chambers (Table 2). For the tests using an initial TAN concentration in the feed of 2.4, 5.2, 7.1 and 10.6 g N/L, the R^2 values for TAN in the feed were 0.997, 0.996, 0.995 and 0.996, respectively. High R^2 values were also obtained for the volume and trapping solution data, indicating the accuracy of the proposed model. Overall, the satisfactory fitting results for the different concentrations of feed solutions indicated that the model could reliably simulate the behavior of GPM contactor across a broad range of operational conditions.

Table 1
Estimated K_m values from the model without water transport at different feed solution TAN concentrations.

Feed TAN conc.	2.4 g N/L	5.2 g N/L	7.1 g N/L	10.6 g N/L
K_m (10^{-7}m/s)	9.7 ± 0.5	5.8 ± 0.3	5.0 ± 0.3	6.9 ± 0.4
R^2, TAN in feed	0.996	0.995	0.995	0.995

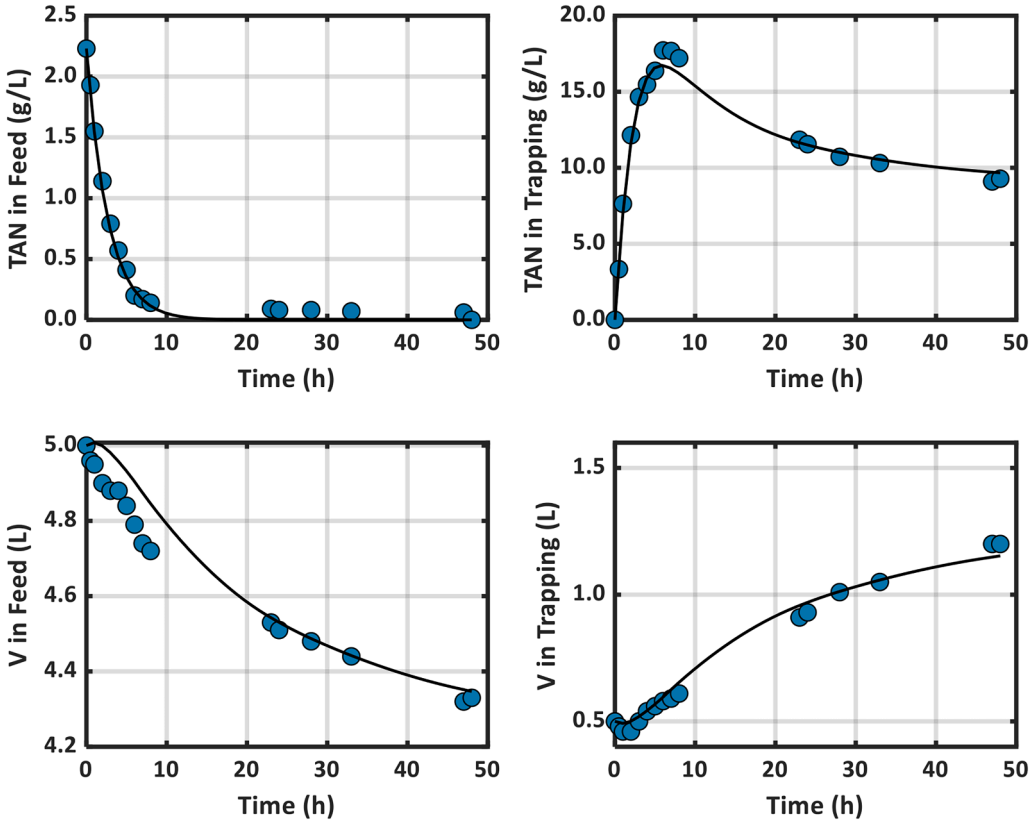

Fig. 4. Fitting results of experimental data (dots) using the new model with water transport (line) at a feed solution TAN concentration of 2.4 g N/L.

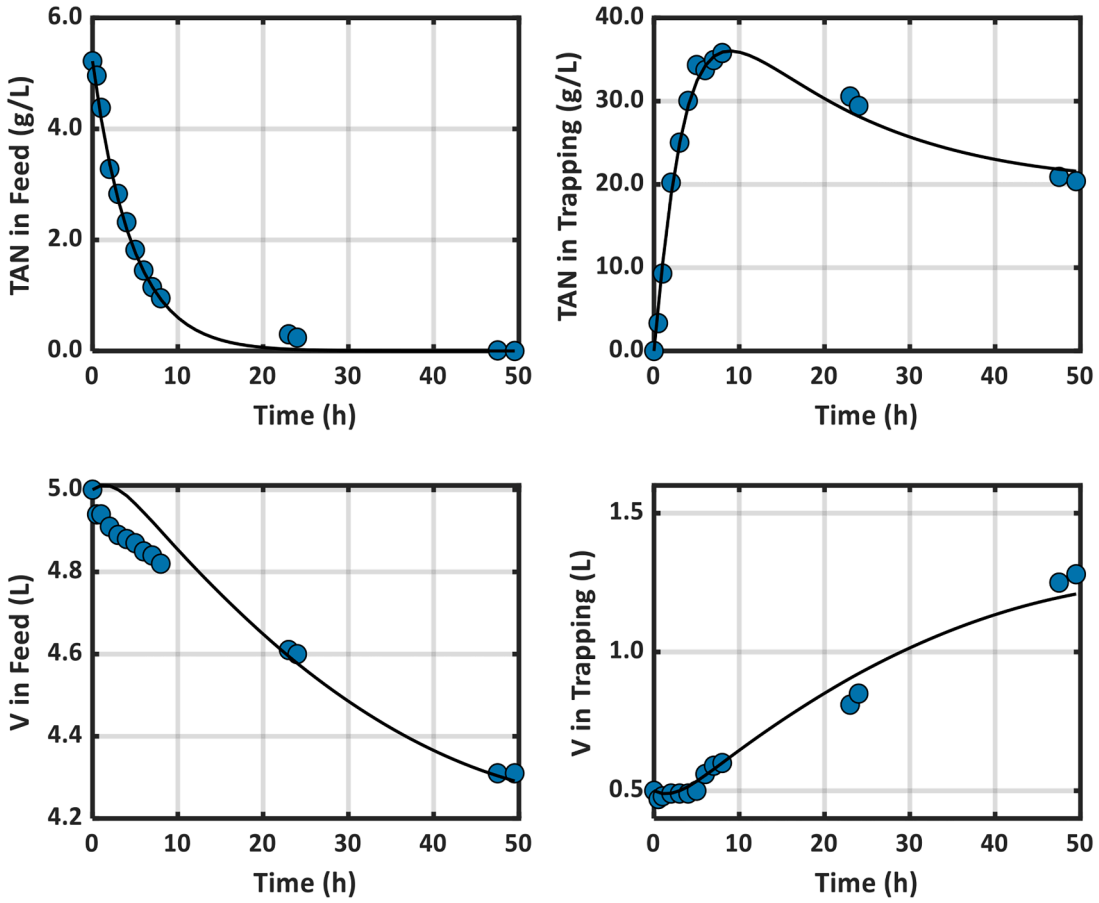

Fig. 5. Fitting results of experimental data (dots) using the new model with water transport (line) at a feed solution TAN concentration 5.2 g N/L.

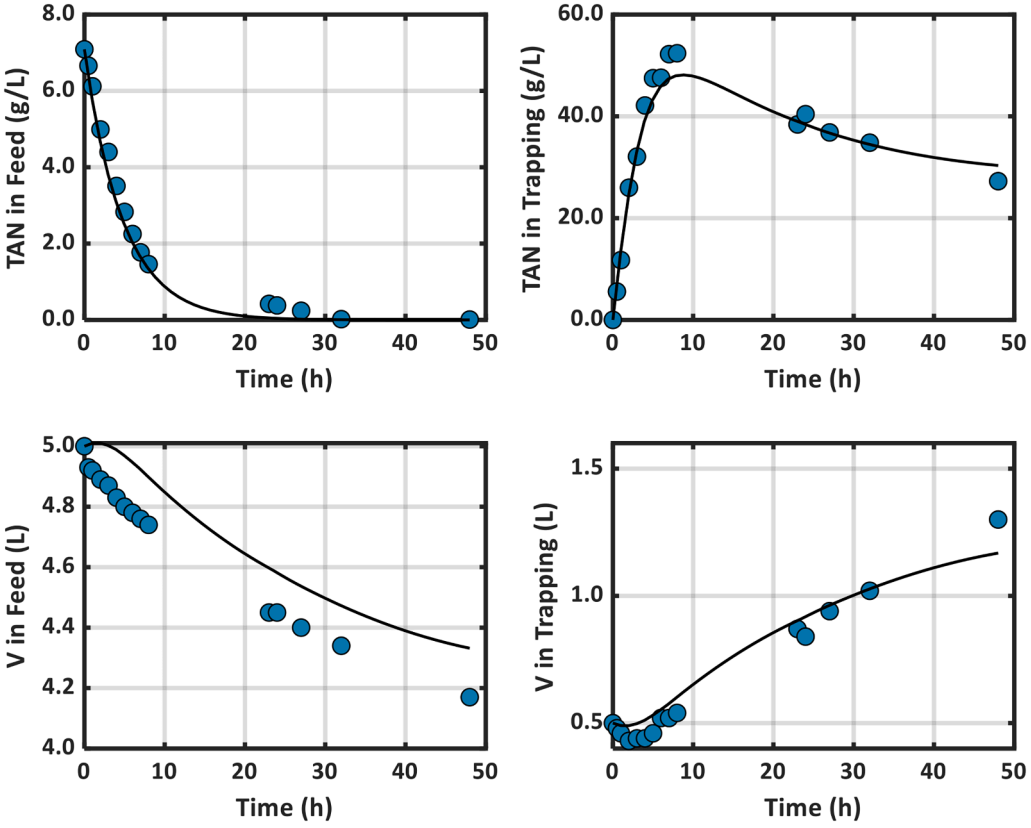

Fig. 6. Fitting results of experimental data (dots) using the new model with water transport (line) at a feed solution TAN concentration of 7.1 g N/L.

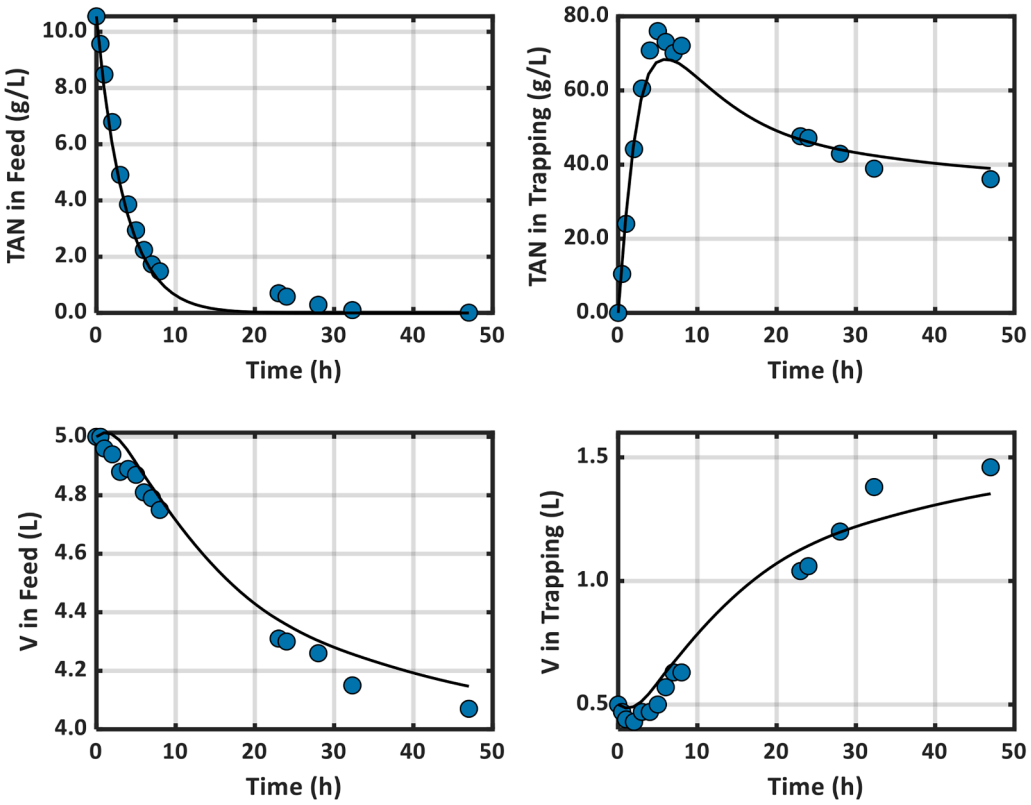

Fig. 7. Fitting results of experimental data (dots) using the new model with water transport (line) at a feed solution TAN concentration of 10.6 g N/L.

Table 2
Transport coefficients (K_m and K_w) and determination coefficients from the new model considering water transport for the experiments carried out at different feed solution TAN concentrations.

Experiment	2.4 g N/L	5.2 g N/L	7.1 g N/L	10.6 g N/L
K_m (10^{-6} m/s)	2.06 ± 0.09	1.20 ± 0.04	1.17 ± 0.07	1.57 ± 0.09
K_w (10^{-10} m/(s bar))	8.24 ± 0.30	3.38 ± 0.16	2.40 ± 0.14	2.78 ± 0.14
R^2, TAN in feed	0.997	0.996	0.995	0.996
R^2, TAN in trapping	0.987	0.989	0.978	0.975
R^2, V in feed	0.959	0.946	0.969	0.993
R^2, V in trapping	0.989	0.977	0.964	0.966

3.3. Potential and limitations of the new model

Modeling nitrogen transport in a gas-permeable membrane while considering water transport offers a significant advantage over the conventional model that does not consider water transport. Water transport dilutes the trapping solution, creating an economic challenge by hindering the goal of achieving a concentrated nitrogen solution. Another advantage of the new model is using osmotic pressure instead of vapor pressure as a variable to model water transport across the membrane, since osmotic pressure can be experimentally measured using an osmometer. This would enable the application and extension of this modeling approach to real wastewater systems in which it is not possible to measure all the dissolved species to predict the osmotic pressure. Some studies have predicted vapor pressure of water (Gonzalez-Salgado et al., 2023; Sheikh et al., 2023; Zhu et al., 2024). However, the necessary correlations to assess the activity water coefficient are still scarce (Sheikh et al., 2023). Moreover, measuring vapor pressure directly in an experimental setting could be complex and challenging. Osmotic pressure measurements could provide a more practical and cost-effective alternative, facilitating the modeling of water diffusion in real conditions.

Although a wide range of initial TAN concentrations were tested, this model has been applied to the treatment of synthetic wastewater where all the present chemical compounds were known. Therefore, more research is needed to validate the model using real wastewater to ensure its applicability in complex matrices. Additionally, the conventional model does not consider a potential decrease in TAN recovery due to membrane wetting and/or fouling over time. These factors would surely impact the long-term performance and reliability of the gas-permeable membrane process. Despite these limitations, the model's ability to simulate TAN recovery and water transport accurately provides a robust foundation for further refinement. Future work should focus on validating the model with real wastewater and incorporating factors such as membrane fouling and wetting into the transport constants to enhance the model's predictive power and reliability.

4. Conclusions

A new model was developed to simultaneously simulate the dynamics of ammonia and water diffusion across the membrane, where osmotic pressure was used as driving force for water diffusion. The developed model successfully simulates the behavior of ammonia transfer (K_m ranging from $1.17{\cdot}10^{-6}$ to $2.06{\cdot}10^{-6}$ m/s) and water transfer (K_w ranging from $2.40{\cdot}10^{-10}$ to $8.24{\cdot}10^{-10}$ m/(s bar)). High R^2 values in the model fitting indicate that it accurately captures the dynamics of the system across different operational conditions. This novel model provides a practical and measurable approach to predict both water transport and nitrogen recovery in real wastewater systems. The average

water fluxes from this study were 0.026, 0.028, 0.027 and 0.035 kg/(m^2 h) for experiments carried out at 2.4, 5.2, 7.1 and 10.6 g N/L, respectively. These water fluxes are lower than those reported in the literature which can be related to the hydrophobicity of the membrane. Overall, simultaneously modeling nitrogen transport and water transport provides a key advantage over the conventional model, as water transport dilutes the trapping solution, limiting TAN accumulation and lowering its commercial value.

CRediT authorship contribution statement

C. Da Silva: Writing – original draft, Visualization, Software, Methodology, Formal analysis, Conceptualization. **A. Serra-Toro:** Writing – original draft, Visualization, Methodology, Investigation, Data curation, Conceptualization. **V. Pelizzaro:** Writing – review & editing, Investigation. **F. Valentino:** Writing – review & editing, Formal analysis. **S. Astals:** Writing – review & editing, Supervision, Funding acquisition. **F. Mas:** Writing – review & editing, Supervision, Funding acquisition, Data curation, Conceptualization. **J. Dosta:** Writing – review & editing, Supervision, Funding acquisition, Conceptualization.

Declaration of competing interest

The authors declare that they have no known competing financial interests or personal relationships that could have appeared to influence the work reported in this paper.

Acknowledgments

This work is supported by the Spanish Ministry of Science, Innovation and Universities (TED2021-132422B-I00 and PID2022-142023OB-I00). Andreu Serra-Toro is grateful to the Spanish Ministry of Science, Innovation and Universities for his FPI grant (PREP2022-000850). Cristopher Da Silva is grateful to Agència de Gestió d'Ajuts Universitaris i de Recerca (AGAUR) de Catalunya for his predoctoral grant (2020 FISDUR 00554). The authors also wish to thank the Institut de l'Aigua of University of Barcelona for their financial support. Francesc Mas acknowledges the financial support of the Spanish Structures of Excellence Maria de Maeztu program (CEX2021-001202-M). The authors would like to thank the Catalan Government for the quality accreditation given to both research groups of the University of Barcelona (2021 SGR 00234 and 2021 SGR 00350).

Supplementary materials

Supplementary material associated with this article can be found, in the online version, at doi:10.1016/j.watres.2024.122771.

Data availability

The data that has been used is confidential.

References

Aguilar-Pozo, V.B., Chimenos, J.M., Elduayen-Echave, B., Olaciregui-Arizmendi, K., López, A., Gómez, J., Guembe, M., García, I., Ayesa, E., Astals, S., 2023. Struvite precipitation in wastewater treatment plants anaerobic digestion supernatants using a magnesium oxide by-product. Sci. Total Environ. 890, 164084. https://doi.org/10.1016/j.scitotenv.2023.164084.

Al-Juboori, R.A., Al-Shaeli, M., Aani, S.A., Johnson, D., Hilal, N., 2023. Membrane technologies for nitrogen recovery from waste streams: scientometrics and technical analysis. Membranes 13, 15. https://doi.org/10.3390/membranes13010015.

Al-Juboori, R.A., Uzkurt Kaljunen, J., Righetto, I., Mikola, A., 2022. Membrane contactor onsite piloting for nutrient recovery from mesophilic digester reject water: the effect of process conditions and pre-treatment options. Sep. Purif. Technol. 303, 122250. https://doi.org/10.1016/j.seppur.2022.122250.

Atkins, P., Paula, J.D., Keeler, J., 2022. Atkins' Physical Chemistry, 12th ed. Oxford University Press. https://doi.org/10.1093/hesc/9780198847816.001.0001.

Baker, W.R., 2023. Membrane Technology and Applications, 4th ed. John Wiley & Sons.

Beckinghausen, A., Odlare, M., Thorin, E., Schwede, S., 2020. From removal to recovery: an evaluation of nitrogen recovery techniques from wastewater. Appl. Energy 263, 114616. https://doi.org/10.1016/j.apenergy.2020.114616.

Berk, Z., 2009. Chapter 10 - Membrane processes. In: Berk, Z. (Ed.), Food Process Engineering and Technology, Food Science and Technology. Academic Press, San Diego, pp. 233–257. https://doi.org/10.1016/B978-0-12-373660-4.00010-7.

Daguerre-Martini, S., Vanotti, M.B., Rodriguez-Pastor, M., Rosal, A., Moral, R., 2018. Nitrogen recovery from wastewater using gas-permeable membranes: impact of inorganic carbon content and natural organic matter. Water Res. 137, 201–210. https://doi.org/10.1016/j.watres.2018.03.013.

Darestani, M., Haigh, V., Couperthwaite, S.J., Millar, G.J., Nghiem, L.D., 2017. Hollow fibre membrane contactors for ammonia recovery: current status and future developments. J. Environ. Chem. Eng. 5, 1349–1359. https://doi.org/10.1016/j.jece.2017.02.016.

de Vries, W., 2021. Impacts of nitrogen emissions on ecosystems and human health: a mini review. Curr. Opin. Environ. Sci. Health 21, 100249. https://doi.org/10.1016/j.coesh.2021.100249.

Dube, P.J., Vanotti, M.B., Szogi, A.A., García-González, M.C., 2016. Enhancing recovery of ammonia from swine manure anaerobic digester effluent using gas-permeable membrane technology. Waste Manag. 49, 372–377. https://doi.org/10.1016/j.wasman.2015.12.011.

Fillingham, M., VanderZaag, A., Singh, J., Burtt, S., Crolla, A., Kinsley, C., MacDonald, J. D., 2017. Characterizing the performance of gas-permeable membranes as an ammonia recovery strategy from anaerobically digested dairy manure. Membranes 7, 59. https://doi.org/10.3390/membranes7040059.

Gonzalez-Salgado, I., Bounouba, M., Dubos, S., Mengelle, E., Guigui, C., Sperandio, M., 2023. Influence of feed salinity on ammonia recovery from high-strength effluents in transmembrane chemical absorption process. J. Membr. Sci. 687, 122086. https://doi.org/10.1016/j.memsci.2023.122086.

Li, X.-M., Reinhoudt, D., Crego-Calama, M., 2007. What do we need for a superhydrophobic surface? A review on the recent progress in the preparation of superhydrophobic surfaces. Chem. Soc. Rev. 36, 1350. https://doi.org/10.1039/b602486f.

Licon Bernal, E.E., Maya, C., Valderrama, C., Cortina, J.L., 2016. Valorization of ammonia concentrates from treated urban wastewater using liquid–liquid membrane contactors. Chem. Eng. J. 302, 641–649. https://doi.org/10.1016/j.cej.2016.05.094.

Marler, R.T., Arora, J.S., 2010. The weighted sum method for multi-objective optimization: new insights. Struct. Multidiscip. Optim. 41, 853–862. https://doi.org/10.1007/s00158-009-0460-7.

Mosadegh-Sedghi, S., Rodrigue, D., Brisson, J., Iliuta, M.C., 2014. Wetting phenomenon in membrane contactors – Causes and prevention. J. Membr. Sci. 452, 332–353. https://doi.org/10.1016/j.memsci.2013.09.055.

Munasinghe-Arachchige, S.P., Abeysiriwardana-Arachchige, I.S.A., Delanka-Pedige, H. M.K., Cooke, P., Nirmalakhandan, N., 2021. Nitrogen-fertilizer recovery from urban sewage via gas permeable membrane: process analysis, modeling, and intensification. Chem. Eng. J. 411, 128443. https://doi.org/10.1016/j.cej.2021.128443.

Norddahl, B., Horn, V.G., Larsson, M., du Preez, J.H., Christensen, K., 2006. A membrane contactor for ammonia stripping, pilot scale experience and modeling. Desalination 199, 172–174. https://doi.org/10.1016/j.desal.2006.03.037. Euromembrane 2006.

Noriega-Hevia, G., Serralta, J., Borrás, L., Seco, A., Ferrer, J., 2020. Nitrogen recovery using a membrane contactor: modelling nitrogen and pH evolution. J. Environ. Chem. Eng. 8, 103880. https://doi.org/10.1016/j.jece.2020.103880.

Noriega-Hevia, G., Serralta, J., Seco, A., Ferrer, J., 2023. A pH-based control system for nitrogen recovery using hollow fibre membrane contactors. J. Environ. Chem. Eng. 11, 110519. https://doi.org/10.1016/j.jece.2023.110519.

Ott, J.B., Boerio-Goates, J., 2000. Chapter 18 - Applications of thermodynamics to solutions containing electrolyte solutes. In: Ott, J.B., Boerio-Goates, J. (Eds.), Chemical Thermodynamics: Advanced Applications. Academic Press, London, pp. 309–358. https://doi.org/10.1016/B978-012530985-1.50009-6.

Perez-Esteban, N., Vives-Egea, J., Peces, M., Dosta, J., Astals, S., 2024. Temperature-driven carboxylic acid production from waste activated sludge and food waste: co-fermentation performance and microbial dynamics. Waste Manag. 178, 176–185. https://doi.org/10.1016/j.wasman.2024.02.026.

Riaño, B., Molinuevo-Salces, B., Vanotti, M.B., García-González, M.C., 2019. Application of gas-permeable membranes for-semi-continuous ammonia recovery from swine manure. Environments 6, 32. https://doi.org/10.3390/environments6030032.

Rizzioli, F., Bertasini, D., Bolzonella, D., Frison, N., Battista, F., 2023. A critical review on the techno-economic feasibility of nutrients recovery from anaerobic digestate in the agricultural sector. Sep. Purif. Technol. 306, 122690. https://doi.org/10.1016/j.seppur.2022.122690.

Rongwong, W., Sairiam, S., 2020. A modeling study on the effects of pH and partial wetting on the removal of ammonia nitrogen from wastewater by membrane contactors. J. Environ. Chem. Eng. 8, 104240. https://doi.org/10.1016/j.jece.2020.104240.

Serra-Toro, A., Abboud, Y.B.H., Cardete-Garcia, M.A., Astals, S., Valentino, F., Mas, F., Dosta, J., 2024. Ammoniacal nitrogen recovery from swine slurry using a gas-permeable membrane: pH control strategies and feed-to-trapping volume ratio. Environ. Sci. Pollut. Res. https://doi.org/10.1007/s11356-024-32193-5.

Serra-Toro, Andreu, Astals, S., Madurga, S., Mata-Álvarez, J., Mas, F., Dosta, J., 2022a. Ammoniacal nitrogen recovery from pig slurry using a novel hydrophobic/hydrophilic selective membrane. J. Environ. Chem. Eng. 10, 108434. https://doi.org/10.1016/j.jece.2022.108434.

Serra-Toro, A., Vinardell, S., Astals, S., Madurga, S., Llorens, J., Mata-Álvarez, J., Mas, F., Dosta, J., 2022b. Ammonia recovery from acidogenic fermentation effluents using a

gas-permeable membrane contactor. Bioresour. Technol. 356, 127273. https://doi.org/10.1016/j.biortech.2022.127273.

Sheikh, M., Lopez, J., Reig, M., Vecino, X., Rezakazemi, M., Valderrama, C.A., Cortina, J. L., 2023. Ammonia recovery from municipal wastewater using hybrid NaOH closed-loop membrane contactor and ion exchange system. Chem. Eng. J. 465, 142859. https://doi.org/10.1016/j.cej.2023.142859.

Soto, R., Fité, C., Ramírez, E., Bringué, R., Cunill, F., 2017. Kinetic modeling of the simultaneous etherification of ethanol with C4 and C5 olefins over Amberlyst™ 35 using model averaging. Chem. Eng. J. 307, 122–134. https://doi.org/10.1016/j.cej.2016.08.038.

Tchobanoglous, G., Stensel, H.D., Tsuchihashi, R., Burton, F.L., Abu-Orf, M., Bowden, G., Pfrang, W., 2014. Wastewater engineering: Treatment and Resource Recovery, 5th ed. McGraw-Hill Education, New York, NY.

Tesser, R., Russo, V., 2020. Advanced Reactor Modeling With MATLAB: Case Studies With Solved Examples. De Gruyter. https://doi.org/10.1515/9783110632927.

Vecino, X., Reig, M., Bhushan, B., Gibert, O., Valderrama, C., Cortina, J.L., 2019. Liquid fertilizer production by ammonia recovery from treated ammonia-rich regenerated streams using liquid-liquid membrane contactors. Chem. Eng. J. 360, 890–899. https://doi.org/10.1016/j.cej.2018.12.004.

Xie, M., Shon, H.K., Gray, S.R., Elimelech, M., 2016. Membrane-based processes for wastewater nutrient recovery: technology, challenges, and future direction. Water Res. 89, 210–221. https://doi.org/10.1016/j.watres.2015.11.045.

Zhang, J., Xie, M., Tong, X., Liu, S., Qu, D., Xiao, S., 2020. Recovery of ammonium nitrogen from human urine by an open-loop hollow fiber membrane contactor. Sep. Purif. Technol. 239, 116579. https://doi.org/10.1016/j.seppur.2020.116579.

Zhu, Y., Chang, H., Yan, Z., Liu, C., Liang, Y., Qu, F., Liang, H., Vidic, R.D., 2024. Review of ammonia recovery and removal from wastewater using hydrophobic membrane distillation and membrane contactor. Sep. Purif. Technol. 328, 125094. https://doi.org/10.1016/j.seppur.2023.125094.

Zhu, Z., Hao, Z., Shen, Z., Chen, J., 2005. Modified modeling of the effect of pH and viscosity on the mass transfer in hydrophobic hollow fiber membrane contactors. J. Membr. Sci. 250, 269–276. https://doi.org/10.1016/j.memsci.2004.10.031.